SCIENTIFIC PAPER
Published: March 19, 2026
https://doi.org/10.13167/2026.32.5

Mechanical properties and flexural behaviour evaluation of ultra-high-performance concrete using hybrid natural fibres

Ananthakumar Ayyadurai[1]✉, Saravanan Marudai Muthuchamy[1], Dineshkumar Gopalakrishnan[2], Maniarasan Settiannan Karuppannan[3] and Miyalvaganan Raju[4]

[1] *Vivekanandha College of Engineering for Women, Department of Civil Engineering, Tiruchengode, 637205, Tamilnadu, India*

[2] *Vaagdevi College of Engineering, Department of Civil Engineering, Bollikunta, 506005, Warangal, India*

[3] *Kongu Engineering College, Department of Architecture, Erode, 638060, Tamilnadu, India*

[4] *Vivekanandha Institute of Information and Management Studies, Department of Master of Business Administration, Tiruchengode, 637205, Tamilnadu, India*

Corresponding author:
Ananthakumar Ayyadurai

Received:
July 14, 2025

Revised:
December 29, 2025

Accepted:
February 2, 2026

Published:
March 19, 2026

Citation:
Ayyadurai, A. et al. Mechanical properties and flexural behaviour evaluation of ultra-high-performance concrete using hybrid natural fibres. *Advances in Civil and Architectural Engineering,* 2026, 17 (32), pp. 75-96. https://doi.org/10.13167/2026.32.5

ADVANCES IN CIVIL AND ARCHITECTURAL ENGINEERING (ISSN 2975-3848)

Faculty of Civil Engineering and Architecture Osijek
Josip Juraj Strossmayer University of Osijek
Vladimira Preloga 3
31000 Osijek
CROATIA

Abstract:
This study aimed to elucidate the effects of incorporating basalt and banana fibres on the mechanical behaviour of ultra-high-performance concrete (UHPC). Two distinct UHPC groups were evaluated; the first group consisted of unreinforced control specimens, whereas the second group included fibre-reinforced specimens with systematically varied fibre volume fractions of 0,25; 0,50; and 1,00 % to assess the impact of fibre content. The fibres enabled a thorough assessment of their types and impact on UHPC performance. Beam-shaped specimens were cast with these fibre contents to facilitate three-point bending tests, enabling assessment of their response under flexural loading. The results conclusively demonstrate that incorporating 1,00 % basalt fibres yielded significantly improved performance compared to all other mix proportions, including those containing banana fibres or lower basalt fibre content. This outcome highlights the potential of basalt fibres as a valuable reinforcement strategy for enhancing the mechanical properties of UHPC, particularly its flexural resistance and energy-dissipation capabilities.

Keywords:
basalt fibre; banana fibre; ultra-high-performance-concrete; mechanical properties; fracture energy

1 Introduction

Concrete is a ubiquitous construction material that has shaped the built environment for millennia. Its versatility, durability, and affordability have solidified its place as the cornerstone of infrastructure and buildings. However, inherent limitations, such as brittleness and susceptibility to cracking, require continuous advancements. In recent years, fibre-reinforced concrete (FRC) has emerged as a transformative technology that addresses these shortcomings and introduces a new era of possibilities for improved concrete performance. In this study, the structural behaviour of FRC under beam flexural loading was investigated. In conventional concrete, durability factors are inferior under various climatic conditions. Although conventional concrete has numerous advantages, its susceptibility to cracking remains a significant challenge, particularly under harsh climatic conditions. Various approaches have been explored to address these limitations. One promising solution is FRC. FRC directly incorporates different fibre types–steel, natural, or synthetic–into a concrete mixture. These dispersed fibres act as reinforcement systems, effectively mitigating the inherent brittleness of plain concrete. When cracks are initiated, the fibres bridge them, arrest their growth, and enhance the overall toughness and resilience of the concrete structure.

The incorporation of banana fibre (BSF) and coir fibre (CF) alongside alccofine (a limestone filler) improved the mechanical characteristics of high-strength concrete (HSC) compared to the control mix. Banana fibre (BNF) exhibited a more significant positive impact on the mechanical properties of HSC than CF. The elastic nature of BSF may provide an early warning system for the potential failure of concrete [1]. Natural fibres may be susceptible to degradation due to moisture and alkaline environments, potentially affecting the long-term performance of concrete. Surface-modification techniques for natural fibres can enhance their effectiveness in terms of improving their bonding with the concrete matrix [2]. BSF is emerging as a viable alternative to traditional reinforcement materials in concrete owing to their high tensile strength, good fatigue resistance, and excellent thermal stability. This is attributed to enhanced fibre-matrix bonding due to the removal of the sizing layer [3]. BSF can be incorporated into concrete to enhance its crack resistance and energy-absorption capacity. BNF is a renewable resource, making it an eco-friendly alternative [4]. Plant fibres can improve the crack resistance of HSC by bridging and arresting crack propagation. They might also enhance the energy-absorption capacity of HSC, allowing it to withstand impact and deformation better [5; 6]. Polyvinyle alcohol (PVA) fibres might enhance workability and early-age crack control, while basalt fibres offer long-term durability and potentially higher strength gains [7; 8].

Basalt fibres exhibit good thermal insulation properties, potentially leading to basalt-fibre-reinforced concrete (BFRC) with a lower thermal conductivity than plain concrete. Basalt fibres possess high melting points and good thermal stability [9; 10]. Sisal fibre composites, a natural fibre option, are reinforced with fillers to improve their mechanical properties for lightweight automotive applications [11]. Ramie fibres are natural cellulose-based fibres with good specific strength and biodegradability [12; 13]. Cellulose fibres can bridge and arrest cracks, thereby enhancing the concrete's ability to resist cracking and deformation. Increased toughness and energy absorption. Carbon-fibre-reinforced concrete (CFRC) can absorb more impact energy before failure than plain concrete [14]. Incorporating natural fibres improves the performance under bending loads by delaying crack propagation and potentially increasing the ultimate load-carrying capacity [15]. BSF influences the long-term performance of concrete, thereby arresting cracks. BF can improve the resistance of concrete to cracking, which helps prevent the ingress of detrimental substances [16-19]. This enhances the crack resistance of high-strength fibre-reinforced concrete (HSFRC) by bridging and arresting microcracks. Utilising natural fibres promotes eco-friendly practices in concrete production compared to synthetic fibres [20; 21]. Cellulose fibres improve the crack resistance and energy absorption of HSC by bridging and arresting cracks. They offer higher tensile strength than cellulose fibres, potentially leading to more significant improvements in the compressive and flexural strengths of HSC [22]. Nanosilica can improve the packing density of UHPC matrices, leading to higher

compressive and tensile strengths [23-26]. Combinations of heavyweight aggregates and certain fibre types can yield UHPC with optimal properties for radiation-shielding applications [27]. Fibre-reinforced UHPC can absorb more impact energy before failure, making it suitable for structures requiring high energy-dissipation capacities [28-32]. Research on BF application in hybrid UHPC has demonstrated mechanical properties and microstructural performance enhancements, applicable to the development of green hybrid fibre systems [33-38]. Micro-steel fibre reinforcement in UHPC, the flexural behaviour of micro-steel fibre reinforced in the laboratory, and numerical modelling have also been investigated, applicable to the study of fibre bridging effects and ductility improvements [39].

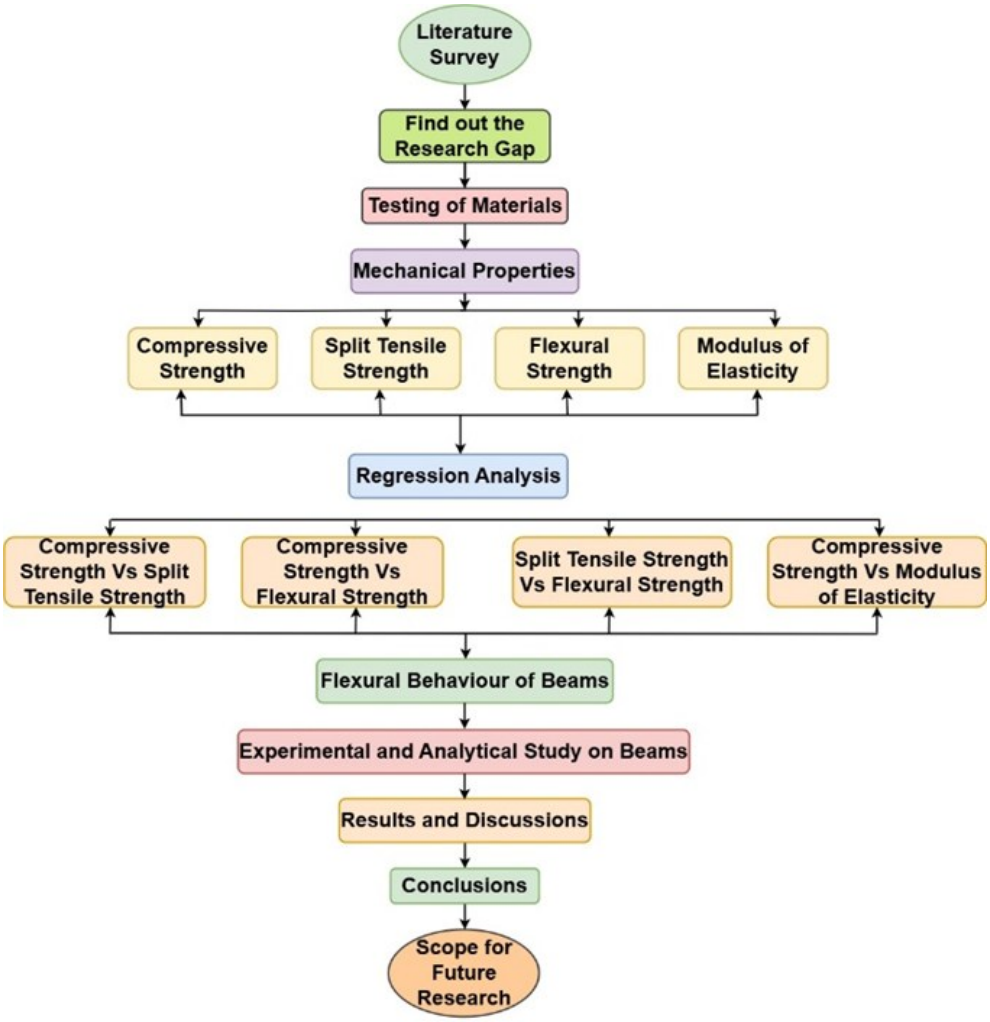

Figure 1. Research methodology flowchart

The mechanical performance of UHPC and UHPFRC with the use of recycled sand has been evaluated, demonstrating promising results for sustainable concrete solutions and high strength [40]. The full-scale production and application of UHPFRC in bridge decks presents information on the practical implementation and structural behaviour of fibre-reinforced UHPC [41]. A review of hybrid fibre compositions in UHPC with a special focus on their implications on the mechanical properties and durability provides a direct basis for the selection of hybrid fibres in this research [42]. The mechanical properties and durability of UHPC reinforced by steel fibres were investigated with a focus on the contribution of fibres to flexibility and tensile performance [43]. Interest in hybrid fibre-reinforced strain-hardening UHPC has grown recently, demonstrating the effects of fibre combinations on the compressive and flexural strengths, applicable to hybrid fibre mix maximisation [44]. Determining the effect of the

material on the UHPC exerted performance provides baseline data and reference mixes to compare fibre-reinforced and hybrid UHPC formulations [45]. Exploring the influence of various fibre types and mixtures on the properties of fresh and hardened UHPC enhances the significance of fibre type and ratio choice [46; 47]. Additionally, the flexural behaviour and ductility of prestressed UHPC beams have been measured, demonstrating failures and structural performance improvements with the addition of fibre reinforcement, which is beneficial when considering the design.

Despite extensive research on the use of synthetic and metallic fibres, such as steel, basalt, and polypropylene, for ultra-high-performance concrete (UHFRC), little effort has been devoted to hybridising inorganic high-strength fibres with biodegradable natural fibres in a UHPC matrix. Although banana fibre has numerous advantages in terms of abundance, cost-effectiveness, and sustainability, it has not been sufficiently explored as a potential structural material in UHPC because of issues associated with durability and bonding at the interface. Furthermore, no systematic experimental investigation has been conducted on the combined utilisation of basalt and banana fibres in UHPC in terms of flexural performance and fracture energy properties.

The current study attempted to fill this research gap. Herein, a new hybrid fibre system that incorporates basalt fibres, owing to their strength and crack-bridging properties, and banana fibres, owing to their energy absorption and sustainability, is proposed. The proposed hybrid fibre system was tested under different fibre ratios. The fibres were added to the concrete mixture at different concentrations, starting with 0,00 % (control group) and increasing in 0,25 percentage increments. Five combinations were tested: 0,00 % fibre (control), 1,00 % basalt fibre only, 0,25 % banana fibre +0,75% basalt fibre, 0,50% each of banana and basalt fibres, and 1,00 % banana fibre only. Through an experimental study of the synergistic impact of basalt–banana fibre hybridisation on flexural behaviour, crack propagation, and fracture energy, the findings of study provide new information on the viability of environmentally friendly fibre hybrid systems in UHPC, enhancing structural performance optimization and sustainable concrete technology. The research workflow is displayed in Figure 1.

2 Materials and methods

2.1 Materials

This study utilized Ordinary Portland cement (CEM I 52,5) and other materials to create the UHPC mixes. Following the PN-EN 197-1:2002 standard, the cement properties were verified (the composition and technical details are provided in Tables 1 and 2, respectively). In addition to cement, the UHPC mixes incorporate micro silica, quartz sand, granite, a superplasticiser, banana fibres, and basalt fibres.

Table 1. Chemical composition of the cement

Component	S_iO_2	Al_2O_3	Fe_2O_3	CaO	MgO	SO_3	Na_2O	K_2O	Cl	LOS	Ash	Total
Content (%)	20,65	3,35	4,28	65,25	1,15	3,10	0,21	0,35	0,078	1,31	0,25	99,97

The particle size distributions of the granite and quartz sand used in the UHPC mixes were determined according to the PN-EN 933-1:2000 standard. The physical and mechanical properties of the coarse aggregates are listed in Table 3. BNFs have a diameter of 20 μm and a length ranging from 12 to 15 mm, with a modulus of elasticity of 27 GPa and a tensile strength of 550 MPa. By contrast, the BSFs are 50 mm long with an aspect ratio of 50, a modulus of elasticity of 85 GPa and a tensile strength of 2600 MPa. Derived from abundant basalt rock, BSFs are environmentally friendly and characterised by energy-efficient production processes and recyclability, contributing to sustainable manufacturing practices. With a moisture content of ≤ 0,10, the concrete mix was enhanced using a superplasticiser based on Sika-Viscocrete-5060.

Table 2. Physical properties of the cement

Cement characteristics	CEM I 52.5N-HSR/NA
Specific surface area (cm^2/g)	4445,00
Water demand (%)	32,00
Commencement of bonding (min)	115,00
End of bonding (min)	175,00
Volume stability according to LeChateliere (mm)	2,00
Compressive strength after 7 days (MPa)	26,50
Compressive strength after 28 days (MPa)	56,80
Tensile strength after 7 days (MPa)	5,37
Tensile strength after 28 days (MPa)	8,35

Table 3. Physical properties of coarse aggregates

Aggregate characteristics	Value
Density (cm^3/g)	2,66
Porosity (%)	0,92
Absorption, W_{24} (%)	0,35
Ash content (%)	0,03
Frost resistance, F (%)	0,17
Resistance to crushing, LA (%)	34,00
Resistance to polishing, PSV (%)	56,00
Shape factor, SI (%)	13,00
Crusher reduction ratio, X_{rm} (%)	14,10
Los Angeles abrasion (%)	15,00

2.2 Mixtures

The concrete mixtures consisted of several components: Portland cement (CEM I 52,5 N-HSR/NA) with a density of 670,5 kg/m^3, granite aggregate (2/8 mm size) at 990 kg/m^3, quartz sand (0/2 mm) at 500 kg/m^3, water (178 l/m^3), silica fume (74,5 kg/m^3), and a superplasticiser (1,08 kg/l at +25 °C). The critical variable between the mixtures was the amount of banana and basalt fibres, expressed as a percentage of the total concrete mix, as reported in Table 4.

Table 4. Fibre percentages of the concrete mixtures

Concrete type	Mass (kN/m^3)		Percentage (%)	
	Basalt fibre BSF	Banana fibre BNF	Basalt fibre BSF	Banana fibre BNF
C	---	---	---	---
BSF	0,235	---	1,00	---
BSBNF1	0,176	0,059	0,75	0,25
BSBNF2	0,118	0,118	0,50	0,50
BSBNF3	0,059	0,176	0,25	0,75
BNF	---	0,235	---	1,00

The concrete was then subjected to meticulous mixing. The measured amounts of coarse aggregates and sand were combined with half of the designated water. The cement, microsilica, and superplasticiser were thoroughly mixed with the remaining water to obtain a uniform blend. Once all components were well integrated, the process transitioned to

incorporating various pre-determined quantities of fibres by hand. Finally, to ensure proper compaction and eliminate air pockets, the uniformly mixed concrete was poured into moulds coated with an anti-adhesive substance and vibrated using a dedicated machine. Strength development in concrete relies on a multistage curing process. After 24 h, the concrete samples were removed from the moulds (demoulding). Subsequently, all specimens were cured for 28 d to evaluate the mechanical properties of the UHPC.

2.3 Mechanical properties of UHPC

In this study, the mechanical properties of UHPC containing different BNF and BSF contents were investigated. The UHPC cubic, cylindrical, and prismatic samples were tested to determine their compressive, split tensile, and flexural strengths. The maximum deflection of Plain Cement Concrete (PCC) was also determined under three-point loading conditions. The experiment also examined how the type and amount of fibre affected the compressive and tensile behaviours and fracture energy of the concrete. The compressive strength is a crucial metric for concrete as it reflects its capacity to withstand compressive loads. In this study, cubic specimens measuring 100 mm on each side were subjected to a compressive strength testing following a 28-d curing period. This curing timeframe allowed the concrete to achieve a significant portion of its potential strength, and the test procedure adhered to the PN-EN 12390-3:2002 standard, ensuring consistency and reliability. The indirect tensile strength, also known as split tensile strength, was evaluated following PN-EN 12390-6:2001. Cylindrical specimens with a diameter of 100 mm and length of 200 mm were cast and cured for 28 d before testing on a compressive testing machine. The flexural tensile strength or three-point bending strength was determined according to EN 12390-5:2009 guidelines. Specimens 100 mm wide, 100 mm deep, and 500 mm long were tested after 28 d of curing. A central load was applied to the specimens, with a support span of 300 mm. The static moduli of elasticity of the cylindrical specimens were measured after the curing process was completed. Testing adhered to the ASTM C469-02:2004 standard and employed an extensometer to gauge the deformations.

2.4 Fracture energy

Following 28 days curing period, notched specimens with dimensions of 1000 × 100 × 150 mm were subjected to three-point bending tests following RILEM TC 89-FMT guidelines, as shown in Figure 2.

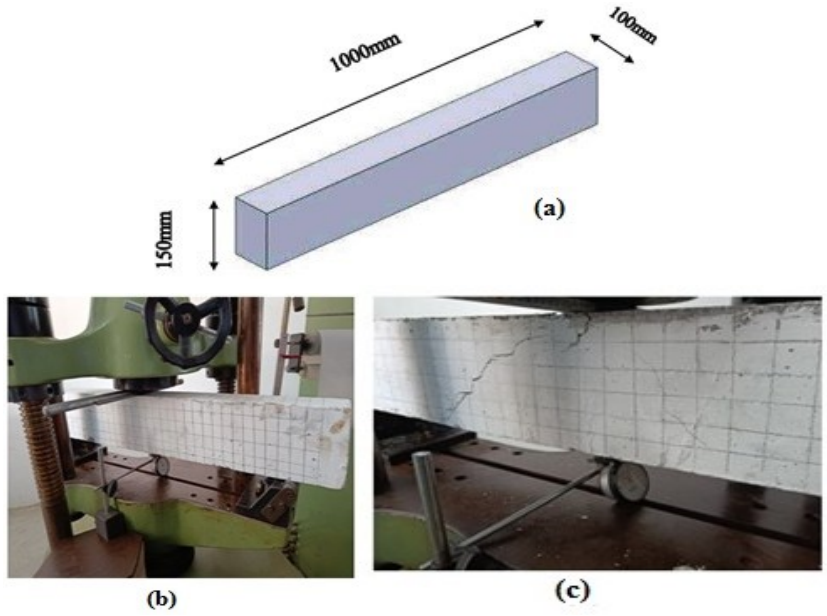

Figure 2. Three-point bending tests on notched specimens: a) geometrical details of the beam; b) test set-up; and c) cracked samples after testing

A constant displacement rate of 0,05 mm/min was applied by using a deflectometer positioned at the base of the specimen. Determining crucial fracture properties, namely, the stress intensity factor (K_{Ic}) and fracture energy (G_F), relied on the established equations referenced in [29] and are presented in Table 5. K_{Ic} characterizes the stress concentration near the crack tip, whereas GF quantifies the energy required for crack propagation. These parameters are critical for modelling the post-cracking stress–strain behaviour of UHPC and fibre-reinforced UHPC. This testing methodology aligns with RILEM recommendation TC162-TDF [30], which acknowledges the influence of the crack mouth opening displacement (CMOD) and fibre distribution on the deflection variability, as supported in the literature [31-33]. The equations for calculating the flexural tensile strength and fracture energy of the fibre-reinforced UHPC are also listed in Table 5.

Table 5. Equations for determining the tensile stress and fracture energy

Type	Strength parameters	Equation
UHPC	Stress intensity factor	$K_{Ic} = \frac{F_{max}}{b\sqrt{h}} f(\alpha)(MN/m^{1.5})$
	Geometry function	$f(a) = 6\sqrt{\alpha}\left(\frac{1{,}99 - \alpha(1-\alpha)(2{,}15 - 3{,}93\alpha + 2{,}7\alpha^2)}{(1+2\alpha)(1-\alpha)^{3/2}}\right)$
	Fracture energy	$G_f = \frac{{K_{Ic}}^2\,(1-v)}{E_{cm}}\ (N/mm)$
Fibre-reinforced UHPC	Tensile stress	$\sigma = \frac{3Fl}{2b(h-a_0)^2}\ (MPa)$
	Fracture energy	$G_f = \int_{\delta=\delta_{lim}}^{\delta=\delta_{lim}} \sigma d\delta (N/mm)$

Where F_{max} denotes critical force; b sample width (b = 100 mm); h sample height (h = 150 mm); α relative crack length ($\alpha = a_0/h$, where a_0 is the notch depth (a_0 = 60 mm)); v Poisson's ratio; E_{cm} average static modulus of elasticity; l sample span (l = 1000 mm); ($h - a_0$) distance between the tip of the notch and the top edge of the sample; and F denotes load recorded during the three-point bending test.

3 Experiments

3.1 Compressive strength

Adding basalt and banana fibres to concrete resulted in changes in properties, with variations observed as the fibre percentage in the concrete mix increased or decreased. Based on the C-S-H gel formation, the bonding behaviour increased compared to that of conventional concrete, indicating improved cohesion. During testing, the cubic specimens experienced damage upon reaching the ultimate load, with fibre-reinforced concrete cubes carrying maximum loads compared to conventional ones. The maximum compressive strength (CS) was achieved with 1 % BSF, with slight variations observed in the specimens containing both basalt and banana fibres (BNBSF), as shown in Figure 3.

However, concrete specimens reinforced with 1 % BNF exhibited lower compressive strengths than those reinforced with conventional concrete. As the percentage increased, BNF led to a 12,6 % strength enhancement in conventional concrete, whereas the BSF specimens exhibited increases of 2,7; 11,8; 20,6; and 55,0 % in compressive strength. However, the BNBSF3 and BNF mixtures exhibited lower compressive strengths than conventional concrete (C).

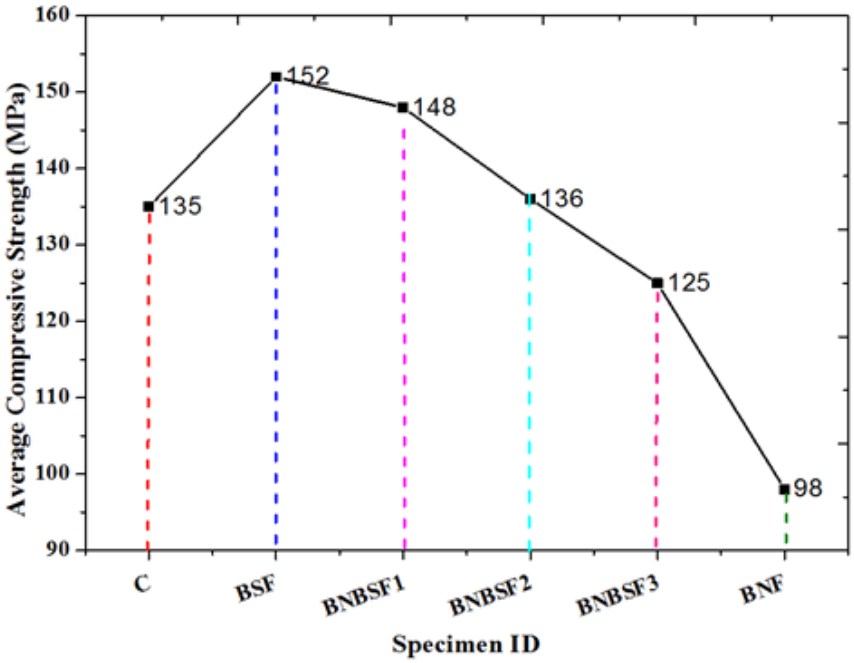

Figure 3. Average compressive strength of all UHPC specimens

3.2 Split tensile strength

According to Figure 4, the average split tensile strength (STS) of the concrete specimens ranged from approximately 5,8 to 10,2 MPa. The 1 % BSF mix achieved the highest STS compared to the other mixtures, whereas the BNF mix exhibited lower STS values than conventional concrete.

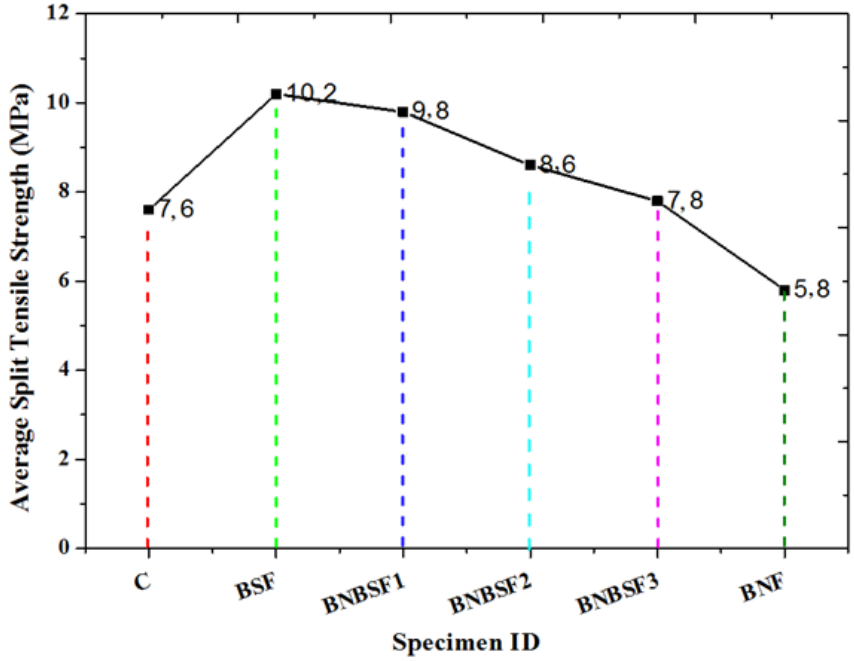

Figure 4. Average split tensile strength of all UHPC specimens

The STS values of the BNBSF1 and BNBSF2 mixtures were slightly closer to the optimum values observed in the BSF mix. The percentage variation in STS depended on the aspect ratio of the basalt and banana fibres. The maximum STS value (10,2 N/mm^2) surpassed that of the other mixtures, including conventional concrete. Mixed BSF increased the split tensile strength by 2,0 % compared to conventional concrete, with increases of 4,1 % for BNBSF1, 18,6 % for BNBSF2, 30,7 % for BNBSF3, and 75,0 % for BNF. The highest percentage increase was observed in the BNBSF3 and BNF mixtures, which was attributed to an increase in the concrete void ratio compared with the optimum mix.

3.3 Flexural strength

Figure 5 shows the average flexural tensile strength values, showing a dependency on the quantities of BNF and BSF in the UHPC. The 1 % BNF mix exhibited the lowest flexural strength compared to the other mixtures, including conventional concrete. Conversely, the highest flexural strength was observed for the 1 % BSF mix, with the BNBSF1 mixture exhibiting a value slightly closer to that of the 1 % BSF mix. Compared with conventional concrete, the BSF mix exhibited a 26 % increase in flexural strength. Furthermore, when compared to BNF, the BSF mix exhibited a notable 58,6 % increase in flexural strength, whereas the BNBSF1, BNBSF2, and BNBSF3 mixtures exhibited increases of 3,0; 12,0; and 17,9 %, respectively.

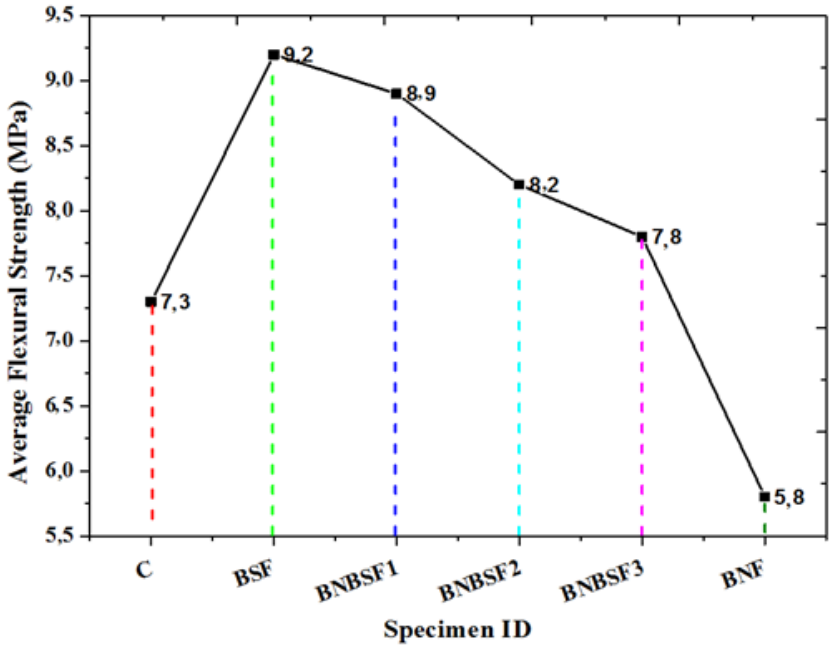

Figure 5. Average flexural strength of all UHPC specimens

3.4 Static modulus of elasticity

The modulus of elasticity (MoE) was determined for both R- and M-sand mixtures using cylindrical specimens with a diameter of 100 mm and a length of 200 mm. The compressive and extensometer devices were affixed to the cylinders and placed on a compression testing machine (CTM) to record the load and deflection data of all samples. The experimental tests were conducted following IS - 516:1959 standards. Figure 6 shows the MoE values of the various concrete mixtures. The BSF mix achieved the highest value (35,24 GPa) compared to the other mixtures. However, the values for the BNBSF2, BNBSF3, and BNF mixtures were lower than that of conventional concrete. The BSF mix exhibited a 5,9 % increase in MoE compared to that of conventional concrete.

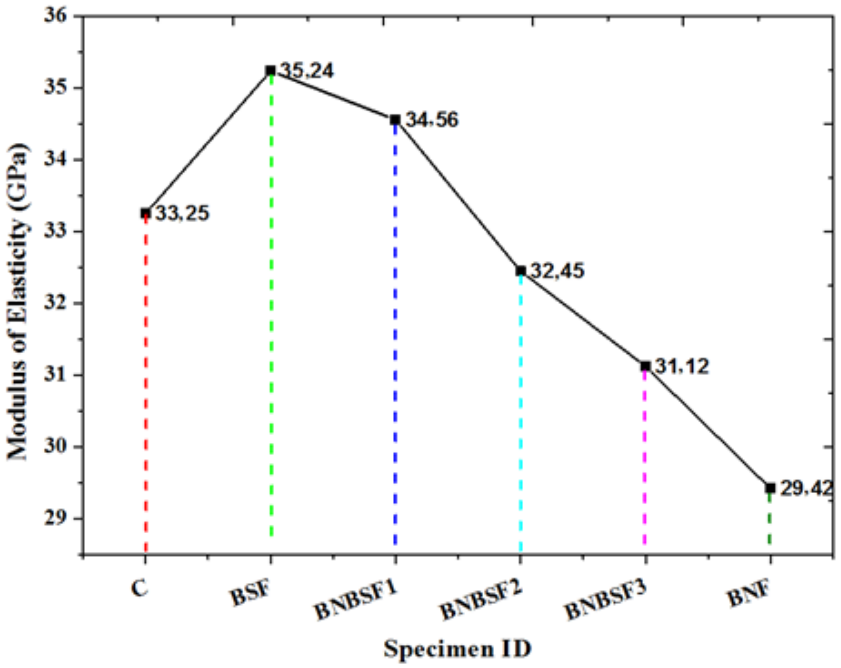

Figure 6. Static modulus of elasticity of all UHPC specimens

3.5 Fracture energy

The evaluation of the equivalent flexural strength and energy required for fracture focused solely on the impact of the fibres. Table 6 displays the average fracture load, deflection, and energy absorption values for UHPC beams with varying fibre contents and microcrack widths.

Table 6. Average UHPC beam structural analysis parameters

Specimen ID	Fibre content (%)	F_{max} (kN)		F_L (kN)	Deflection (mm)		Avg. fracture energy (N/mm)	Avg. micro-crack width (mm)
		Expt.	Anly.		Expt.	Anly.		
CC	0	4,80	4,86	1,2	0,65	0,72	1,152	0,86
BSF	1	6,70	6,84	3,5	3,50	3,57	25,406	0,74
BNBSF1	0,25+0,75	6,30	6,42	3,2	3,25	3,28	25,102	0,89
BNBSF2	0,50+0,50	6,00	6,10	2,8	2,85	2,89	24,840	0,95
BNBSF3	0,75+0,25	5,30	5,34	2,5	2,55	2,61	23,456	1,12
BNF	1	4,30	4,38	3,0	2,30	2,34	20,650	0,84

The control specimen (C) exhibits the lowest average fracture load (4,8 kN) compared to beams incorporating BSF fibres (BNBSF1, BNBSF2, and BNBSF3), with values ranging from 5,3 to 6,0 kN. This indicates a potential enhancement in the overall fracture load capacity of the UHPC beams with the inclusion of BSF. Across all specimens, the average deflection remained consistent at approximately 3 mm, suggesting that BSF addition had a minor impact on the deflection of the UHPC beams under loading. Additionally, the control specimen (C) demonstrates the lowest average energy absorption (0,65 N/mm), while beams with BSF fibres (BNBSF1, BNBSF2, and BNBSF3) exhibit values ranging from 2,30 to 3,50 N/mm. This implies an improvement in the energy-absorption capacity of the UHPC beams owing to the presence of BSF, indicating their ability to withstand higher amounts of energy before fracture.

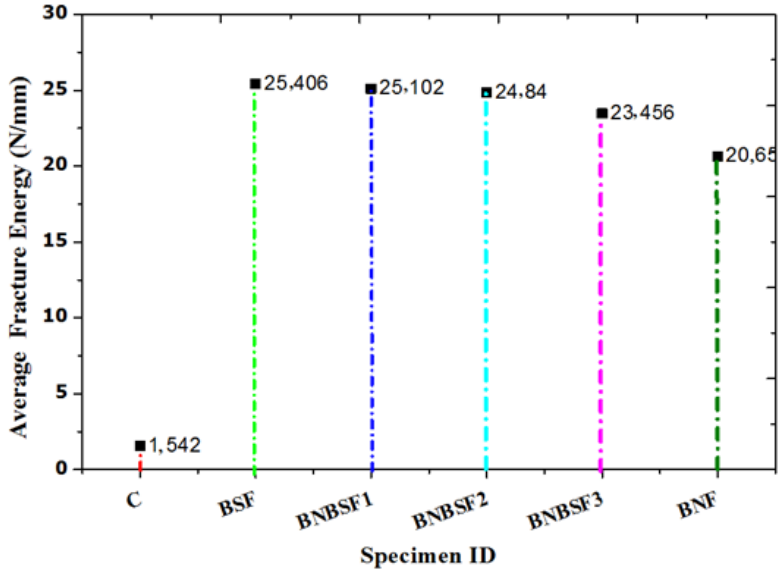

Figure 7. Average fracture energy of all UHPC specimens with and without fibres

Figure 7 shows the average fracture energy of the UHPC specimens with and without fibres. The UHPC specimen without fibres (C) exhibits a significantly lower average fracture energy (approximately 1,5 N/mm) compared to all UHPC specimens with BSF fibres (20,65-25,40 N/mm). This indicates a substantial increase in the fracture energy owing to BSF addition. Among the UHPC specimens with BSF fibres (BNBSF1, BNBSF2, and BNBSF3), minimal variation in the average fracture energy is observed, ranging from 20,650-25,406 N/mm.

The presence of BSF fibres significantly enhances the fracture energy of UHPC specimens compared to those without fibres, highlighting their ability to improve the energy-absorption capacity, as shown in Figure 8. This illustrates the impact of microcracks on the overall performance of the UHPC specimens, which is influenced by their size, distribution, and connectivity. Although more microcracks may initially suggest reduced material robustness, well-distributed and limited-size cracks can be advantageous. Such a network of microcracks can potentially enhance the toughness and energy-absorption capacity of UHPC.

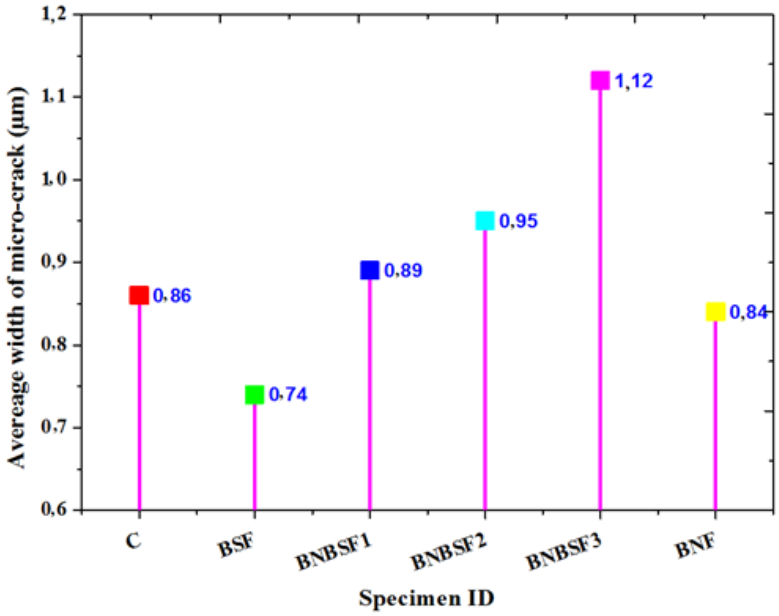

Figure 8. Average micro-crack width variation of all UHPC specimens

3.6 Finite Element Modelling

Finite element modelling (FEM) of the UHPC beams was performed using ANSYS. The 3D model is shown in Figure 9a). A sensitivity analysis was conducted on all UHPC beams to evaluate the effect of mesh size on the results using coarse, medium, and fine meshes, with the fine mesh producing the most accurate results (Figure 9b)). The following key FEM parameters were included: concrete was modelled using a nonlinear concrete damage plasticity model, whereas fibres were represented using embedded truss elements to simulate their reinforcement effect. 3D solid elements were used for the concrete matrix, and truss elements were used for the fibres to capture the fibre–matrix interaction. Loading was applied as a four-point bending, with one end of the beam as a roller support and the other as a hinged support, replicating the experimental setup (Figure 9c)). All UHPC beams were analysed, and the results, including the ultimate deflection and surface stress, are presented in Figures 10 and 11, respectively. The inclusion of these parameters ensured that the FEM results were quantitative, reproducible, and consistent with the experimental observations.

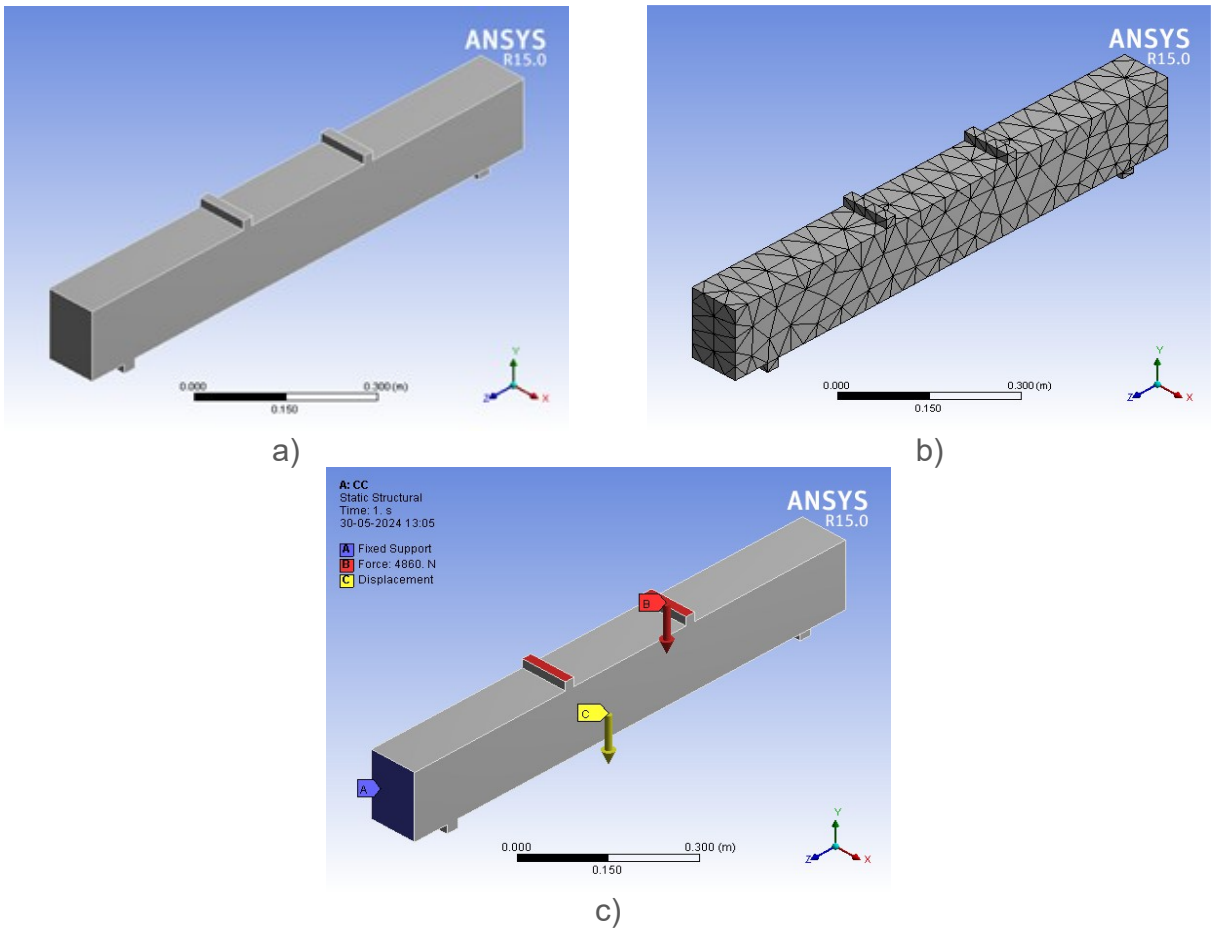

Figure 9. Analytical modelling of the beam: a) 3D beam model; b) beam meshing; and c) beam supporting and loading

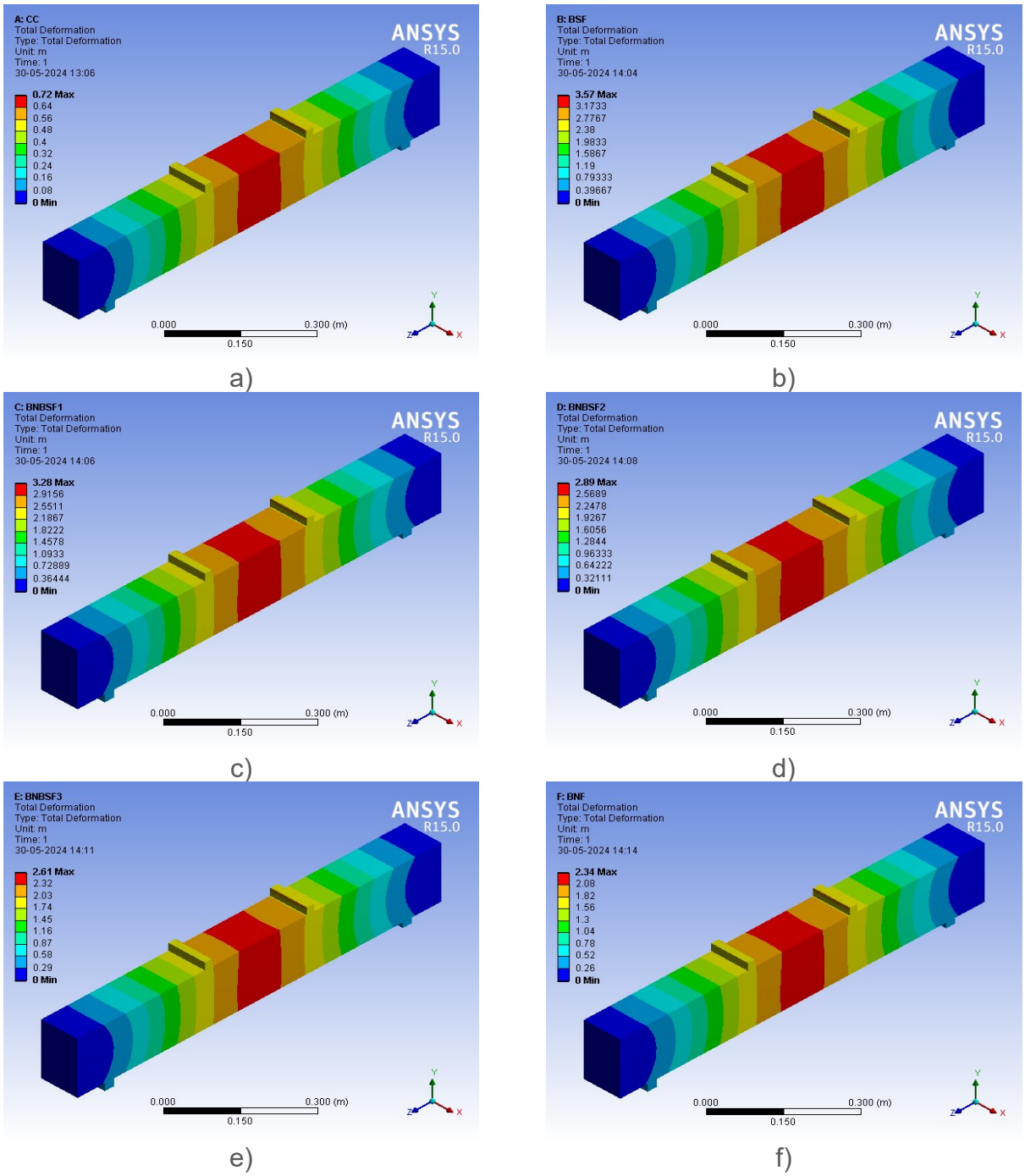

Figure 10. Analytical deflection of the beams: a) C; b) BSF; c) BNBSF1; d) BNBSF2; e) BNBSF3; and f) BNF

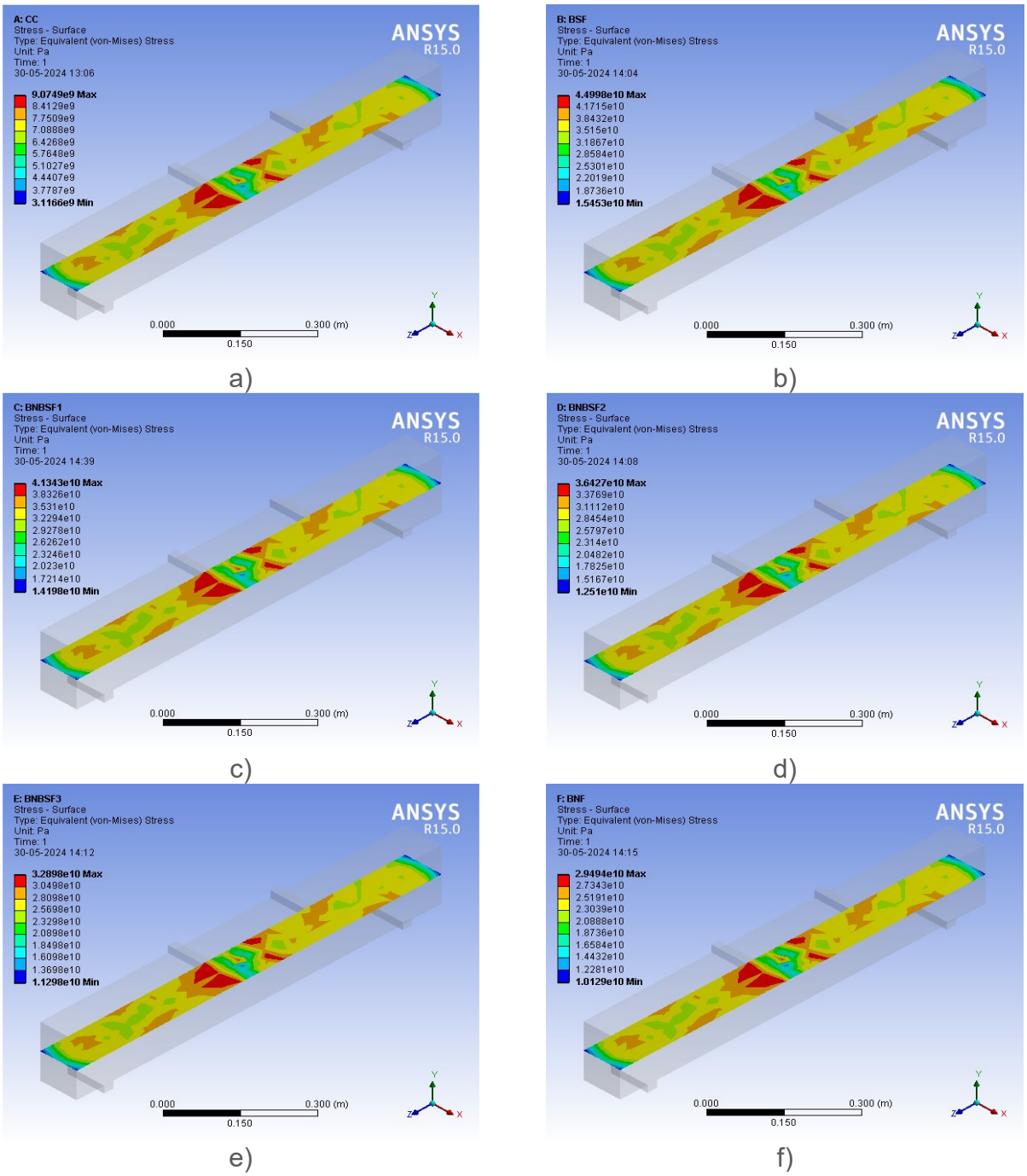

Figure 11. Analytical surface stress of the beams: a) CC; b) BSF; c) BNBSF1; d) BNBSF2; e) BNBSF3; and f) BNF

4 Discussion

4.1 Mechanical properties

The results show the better effectiveness of BSF in terms of enhancing the concrete strength. Based on the test results, dependencies and associations between different concrete properties were proposed. Basalt fibres exhibited superior performance compared with banana fibres because of their higher tensile strength, stiffness, and better bonding with the cementitious matrix, which allowed them to bridge cracks more effectively and resist deformation under loading. By contrast, banana fibres, being natural fibres and less stiff,

contributed primarily to energy absorption but provided limited load-bearing capacity. Figures 12 shows the relationships between fibre concrete's mechanical properties and modulus of elasticity. Figure 12a) represents the relation between the compressive and split tensile strengths of the conventional and fibre variations concrete. The compressive strength of the concrete is directly proportional to its split tensile strength. The polynomial trend was characterized by a good correlation coefficient R^2 = 0,9174 and relatively low errors in the intercept. Split tensile strength = 0,079 × compressive strength – 2,2 represents an empirical relationship obtained through linear regression analysis between the split tensile and compressive strengths. This relationship indicates that for every unit increase in compressive strength, the split tensile strength increases by an average of 0,079 units. This value is much smaller than the flexural strength example (0,60) as concrete is generally much weaker in tension than in compression. Similar to the flexural strength case, this represents (–2,200) the theoretical split tensile strength when the compressive strength is zero, and the flexural strength of the concrete corresponds to its compressive strength, as shown in Figure 12b). The fibre concrete flexural failure mode is less than fibre concrete's compressive strength.

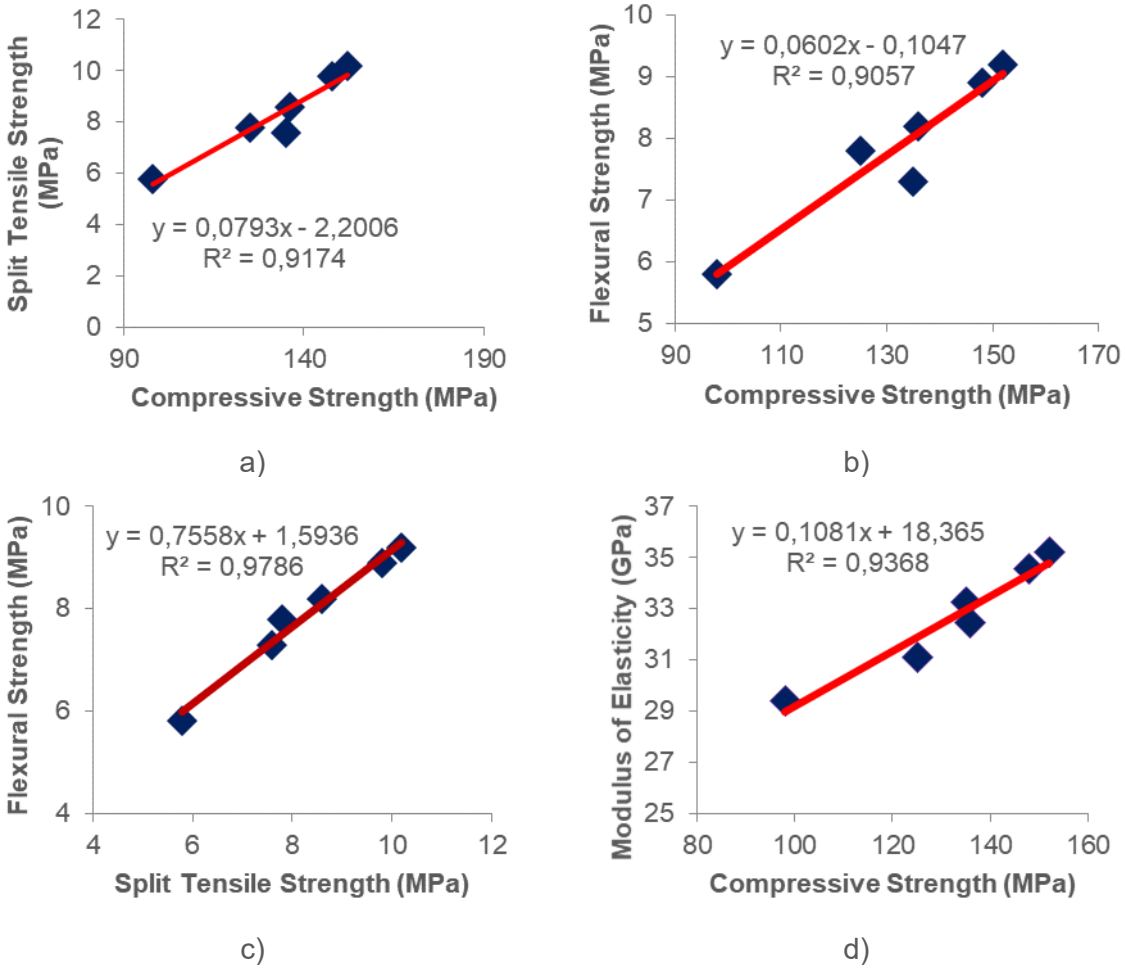

Figure 12. Regression analysis of the UHPC mechanical properties for fibre-reinforced UHPC

The flexural strength of conventional concrete (without fibre) did not correspond to the compressive strength. The R^2 value for the compressive and flexural strength was 0,9057, and the probable equation is FS = 0,60 × CS – 0,104. This coefficient (0,60) indicates that for every unit increase in compressive strength, the average flexural strength increases by 0,6 units, indicating a positive linear correlation between the two. The (–0,104) value represents the

theoretical flexural strength when the compressive strength is zero. In reality, the flexural strength is not harmful, and this value might be due to errors or limitations of the linear model. Figure 12c) shows the relationship between the split tensile and flexural strengths of the fibre concrete. A high correlation coefficient of 0,9786 indicates that the R^2 value matches the data. The equation for flexural strength was 0,755 × STS + 1,593. This coefficient indicates that for every unit increase in split tensile strength, the flexural strength increases by an average of 0,755 units. The positive slope indicates a positive linear correlation between the two strengths (1,593), which represents the theoretical flexural strength when the split tensile strength is zero. In reality, the flexural strength would not be positive without tensile resistance. The modulus of elasticity is directly correlated with the compressive strength of fibre-reinforced concrete. In the linear regression analysis, the R^2 value was 0,9368, as shown in Figure 12d). The probable equation for this coefficient is 0,108 × CS + 18,36. This coefficient indicates that for every unit increase in compressive strength, the modulus of elasticity increases by an average of 0,108 units. The positive slope indicates a positive correlation between the two properties. Materials with higher compressive strengths tended to be stiffer on average. The 18,36 value represents the theoretical modulus of elasticity when the compressive strength is zero. In reality, the modulus of elasticity is not positive without compressive strength. This value arises from the limitations of the linear model and may be influenced by errors in the data used for the regression.

The regression analysis showed strong positive relationships among the mechanical properties of the fibre-reinforced concrete. The compressive strength was closely related to both the split tensile (R^2=0,9174) and flexural strengths (R^2=0,9057), with these strengths exhibiting a very high correlation (R^2=0,9786). The modulus of elasticity also increased with compressive strength (R^2=0,9368). These relationships were statistically validated using the standard error of the estimate, 95 % confidence intervals for the slopes, p-values (< 0,001), and residual analysis, which confirmed that the observed trends were reliable, significant, and consistent with the experimental results.

4.2 Comparison between the experimental and analytical results

The experimental test results for the UHPC beams were compared with the analytical results, as presented in Table 7. The predicted analytical ultimate load and deflection results were highly correlated with the experimental results. The mean ultimate loads and deflections of the UHPC beams were 0,98 and 0,97, respectively. Additionally, the standard deviation values were 0,005 and 0,033 for the ultimate load and deflection, respectively, whereas the R2 values were 0,49 and 3,43, respectively.

Table 7. Comparison between the experimental and analytical results for the UHPC beam specimens

Specimen ID	Fibre content (%)	F_{max} (kN)		Deflection (mm)		Ratio = Expt/Anly	
		Expt.	Anly.	Expt.	Anly	Load	Deflection
CC	0	4,80	4,86	0,65	0,72	0,990	0,900
BSF	1	6,70	6,84	3,50	3,57	0,980	0,980
BNBSF1	0,25+0,75	6,30	6,42	3,25	3,28	0,980	0,990
BNBSF2	0,50+0,50	6,00	6,10	2,85	2,89	0,980	0,990
BNBSF3	0,75+0,25	5,30	5,34	2,55	2,61	0,990	0,980
BNF	1	4,30	4,38	2,30	2,34	0,980	0,980
Mean						0,980	0,970
SD						0,005	0,033
COV						0,490	3,430

4.3 Failure mode

The tested UHPC beams failed under four-point loading; the failure specimens are shown in Figure 13. According to the experiments, the standard failure mode observed for all beams was concrete crushing failure. The control beams failed via concrete crushing, flexural behaviour, and shear failure. Similarly, the addition of banana and basalt fibres to the beams led to an increase in the tensile strength of the specimens. The failure mode of the specimens is commonly divided into three parts, beginning with a load-deflection linear behaviour up to the yield point of the beams [34-37]. In the second stage, the specimens reached the elastic–plastic stage. At this stage, minor cracks propagate throughout the specimens. In the third stage, the specimens failed after reaching their ultimate loads. The ductility and stiffness were determined for all specimens, as reported in Table 8.

Table 8. Ductility, stiffness, and failure mode of the UHPC beam specimens

Specimen ID	Fibre content (%)	Experimental results			Ductility	Stiffness (kN/mm)	Mode of failure
		Ultimate load (kN)	Yield deflection (mm)	Ultimate deflection (mm)			
CC	0	4,80	0,43	0,65	1,51	7,38	CC+FF+SF
BSF	1	6,70	2,14	3,50	1,64	1,91	CC+FF
BNBSF1	0,25+0,75	6,30	2,01	3,25	1,62	1,94	CC+SF+FF
BNBSF2	0,50+0,50	6,00	1,86	2,85	1,53	2,11	CC+SF
BNBSF3	0,75+0,25	5,30	1,74	2,55	1,47	2,08	CC+FF
BNF	1	4,30	1,67	2,30	1,38	1,87	CC+FF+SF

Where SF denotes shear failure; FF flexural failure; and CC concrete crushing.

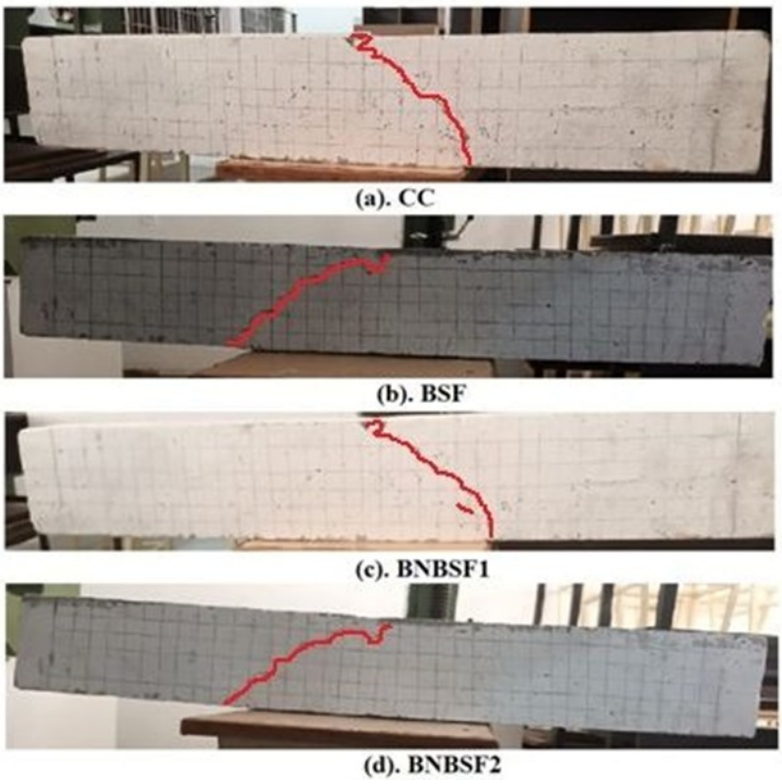

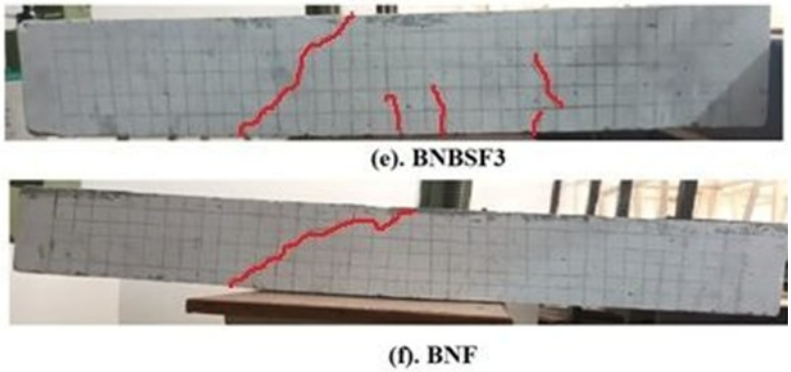

Figure 13. Tested UHPC beam specimens

5 Conclusions

In this study, it was experimentally confirmed that BSF incorporation significantly enhances the mechanical performance of concrete and UHPC compared to conventional concrete and banana-fibre-reinforced mixtures. Among all mixtures, 1 % BSF exhibited the most consistent and superior performance across all evaluated properties.

In terms of compressive strength, the 1 % BSF mix achieved an improvement of up to 55 % compared with plain concrete, demonstrating its effectiveness in enhancing the load-bearing capacity. Although the 1 % BNF mix exhibited a smaller increase (12,6 %), its contribution was comparatively limited, indicating the dominant role of basalt fibres in compressive resistance. The STS results exhibited the highest enhancement for the 1% BSF mix, with an increase of up to 75 % compared with conventional concrete. This improvement reflects the strong fibre–matrix interaction and efficient crack-bridging ability of basalt fibres. The BNF mixtures exhibited marginal improvements, confirming their lower tensile efficiency. The flexural strength of the BSF-reinforced mixtures was notably higher than that of both the control and BNF mixtures, with the 1 % BSF mix achieving a 26 % increase. This indicates improved resistance to bending and delayed crack propagation, whereas the banana fibre mixtures exhibited the least improvement under flexural loading. The modulus of elasticity of the BSF mixtures increased by approximately 5,9 %, indicating enhanced stiffness and reduced deformation under the applied loads. This behaviour supports the suitability of basalt fibres for structural applications requiring higher rigidity. In the UHPC beam tests, BSF significantly improved the fracture load, energy-absorption capacity, and fracture energy. These results confirm the enhanced crack resistance and post-cracking performance, whereas the hybrid BSF–BNF combinations did not exhibit noticeable synergistic benefits. Regression analysis demonstrated strong correlations between compressive strength, split tensile strength, flexural strength, and modulus of elasticity, validating the internal consistency of the experimental results and supporting the predictive relationships between key mechanical properties. Finally, FEM results exhibited close agreement with the experimental observations in terms of the deflection and stress distribution. The numerical model effectively captured the structural response of the UHPC beams, confirming that FEM is a reliable and efficient tool for predicting the experimental behaviour and reducing dependency on extensive physical testing.

Overall, these findings demonstrate that basalt fibres are highly effective in enhancing the strength, stiffness, crack resistance, and fracture performance of UHPC, whereas banana fibres offer only limited benefits and no clear synergistic effect in hybrid combinations. The consistency between the experimental results, regression analysis, and FEM results confirms the robustness of these findings and underscores the potential of basalt-fibre-based UHPC for advanced structural applications, with numerical modelling serving as a cost-efficient approach for design and optimisation.

Future work should focus on fibre parameter optimisation, including the aspect ratio, surface characteristics, and dispersion techniques, to further improve the mechanical and fracture

performance. The validated FEM framework could be extended to reinforced concrete beams and columns under different loading conditions, including cyclic and impact loads, for a more comprehensive structural performance assessment. Further research on the durability performance, including environmental exposure and long-term behaviour, is recommended to evaluate the practical applicability of fibre-reinforced UHPC in real construction scenarios.

Acknowledgments

The authors wish to acknowledge the Department of Civil Engineering, Vivekanandha College of Engineering for Women, Tiruchengode, Tamilnadu, for the facility and support extended to this work.

References

[1] Rajkohila, A.; Prakash Chandar, S.; Ravichandran, P. T. Assessing the effect of natural fiber on mechanical properties and microstructural characteristics of high strength concrete. *Ain Shams Engineering Journal*, 2024, 15 (5), 102666. https://doi.org/10.1016/j.asej.2024.102666

[2] Ilyas, R. A. et al. Crushing and flexural properties of natural fiber-reinforced concrete. *Biocomposites for Industrial Applications*, 2024, pp. 3-28. https://doi.org/10.1016/B978-0-323-91866-4.00002-0

[3] Li, Y.-F. et al. Effect of the sizing removal methods of fiber surface on the mechanical performance of basalt fiber-reinforced concrete. *Fibers*, 2024, 12 (1), 10. https://doi.org/10.3390/fib12010010

[4] Ayyadurai, A.; Muthuchamy Maruthai, S; Muthu, D. Impact of fly ash and banana fiber on mechanical performance of paver block concrete. *Građevinar*, 2024, 76 (3), pp.211-222. https://doi.org/10.14256/JCE.3873.2023

[5] Liu, J.; Liu, X. Fiber-reinforced concrete for complex engineering conditions: material properties, nonlinear response and sustainable applications in spaceflight. *High Temperature Materials and Processes*, 2026, 45 (1), 20250102. https://doi.org/10.1515/htmp-2025-0102

[6] Alomayri, T.; Ali, B. Effect of plant fiber type and content on the strength and durability performance of high-strength concrete. *Construction and Building Materials*, 2023, 394, 132166. https://doi.org/10.1016/j.conbuildmat.2023.132166

[7] Shah, S. H. A. et al. Mechanical performance and environmental impact of normal strength concrete incorporating various levels of coconut fiber and recycled aggregates. *Environmental Science and Pollution Research*, 2022, 29, pp. 83636-83651. https://doi.org/10.1007/s11356-022-21608-w

[8] Shu, Y.; Zhang, J. Effect of basalt fiber content and length on the strength and crack development of polyvinyl alcohol/basalt hybrid fiber-reinforced cement soil. *Polymers*, 2023, 15 (9), 2146. https://doi.org/10.3390/polym15092146

[9] Qsymah, A. et al. Thermal properties, microstructure analysis, and environmental benefits of basalt fiber reinforced concrete. *Journal of Engineered Fibers and Fabrics*, 2023, 18. https://doi.org/10.1177/15589250221146547

[10] Awadeen, M. et al. Mechanical properties, attenuation coefficient, and microstructure of ultra high-performance heavyweight concrete for radiation shielding applications. *Journal of Building Engineering*, 2024, 82, 108395. https://doi.org/10.1016/j.jobe.2023.108395

[11] Miniappan, P. K. et al. Mechanical, fracture-deformation, and tribology behavior of fillers-reinforced sisal fiber composites for lightweight automotive applications. *Reviews on Advanced Materials Science*, 2023, 62 (1), 20230342. https://doi.org/10.1515/rams-2023-0342

[12] Ramesh, V. et al. Influence of stacking sequence on mechanical properties of basalt/ramie biodegradable hybrid polymer composites. *Polymers*, 2023, 15 (4), 985. https://doi.org/10.3390/polym15040985

[13] Qian, Y. et al. Application of machine learning algorithms to evaluate the influence of various parameters on the flexural strength of ultra-high-performance concrete. *Frontiers in Materials*, 2023, 9, 1114510. https://doi.org/10.3389/fmats.2022.1114510
[14] Wu, H. et al. An experimental investigation and optimization of the properties of concrete containing cellulose fiber based on system theory. *Construction and Building Materials*, 2024, 411, 134463. https://doi.org/10.1016/j.conbuildmat.2023.134463
[15] Rajkohila, A.; Chandar, S. P.; Ravichandran, P.T. Flexural performance of HSC beams containing natural fibers. *Journal of Building Pathology and Rehabilitation*, 2024, 9, 71. https://doi.org/10.1007/s41024-024-00423-5
[16] Zeyad, A. M. et al. Effect of aggregate and fibre types on ultra-high-performance concrete designed for radiation shielding. *Journal of Building Engineering*, 2022, 58, 104960. https://doi.org/10.1016/j.jobe.2022.104960
[17] Al-Kharabsheh, B. N. et al. Basalt fiber reinforced concrete: A compressive review on durability aspects. *Materials*, 2023, 16 (1), 429. https://doi.org/10.3390/ma16010429
[18] Lusis, V. et al. Experimental study and modelling on the structural response of fiber reinforced concrete beams. *Applied Sciences*, 2022, 12 (19), 9492. https://doi.org/10.3390/app12199492
[19] Marvila, M. T. et al. Materials for production of high and ultra-high performance concrete: Review and perspective of possible novel materials. *Materials*, 2021, 14 (15), 4304. https://doi.org/10.3390/ma14154304
[20] Adamu, M. et al. A comprehensive review on sustainable natural fiber in cementitious composites: the date palm fiber case. *Sustainability*, 2022, 14 (11), 6691. https://doi.org/10.3390/su14116691
[21] Hasan, M. et al. Mechanical properties and absorption of high-strength fiber-reinforced concrete (HSFRC) with sustainable natural fibers. *Buildings*, 2022, 12 (12), 2262. https://doi.org/10.3390/buildings12122262
[22] Ahmad, J. et al. Improvement in the strength of concrete reinforced with agriculture fibers: Assessment on mechanical properties and microstructure analysis. *Journal of Engineered Fibers and Fabrics*, 2024, 19. https://doi.org/10.1177/15589250241226480
[23] Hakeem, I. Y. et al. Effects of nano-silica and micro-steel fiber on the engineering properties of ultra-high performance concrete. *Structural Engineering and Mechanics*, 2022, 82 (3), pp. 295-312. https://doi.org/10.12989/sem.2022.82.3.295
[24] Abed, S. et al. Influence of ternary hybrid fibers on the mechanical properties of ultrahigh-strength concrete. *Frontiers in Materials*, 2023, 10, 1148589. https://doi.org/10.3389/fmats.2023.1148589
[25] Ahmad, W.; Khan, M.; Smarzewski, P. Effect of short fiber reinforcements on fracture performance of cement-based materials: A systematic review approach. *Materials*, 2021, 14 (7), 1745. https://doi.org/10.3390/ma14071745
[26] Halvaei, M.; Latifi, M.; Jamshidi, M. Study of the microstructure and flexural behavior of cementitious composites reinforced by surface modified carbon textiles. *Construction and Building Materials*, 2018, 158, pp. 243-256. https://doi.org/10.1016/j.conbuildmat.2017.10.044
[27] Zeyad, A. M. et al. Effect of aggregate and fibre types on ultra-high-performance concrete designed for radiation shielding. *Journal of Building Engineering*, 2022, 58, 104960. https://doi.org/10.1016/j.jobe.2022.104960
[28] Yang, J. et al. Effects of fibers on the mechanical properties of UHPC: A review. *Journal of Traffic and Transportation Engineering (English Edition)*, 2022, 9 (3), pp. 363-387. https://doi.org/10.1016/j.jtte.2022.05.001
[29] Kravanja, G.; Mumtaz, A. R.; Kravanja, S. A comprehensive review of the advances, manufacturing, properties, innovations, environmental impact and applications of ultra-high-performance concrete (UHPC). *Buildings*, 2024, 14 (2), 382. https://doi.org/10.3390/buildings14020382

[30] Bandara, S.; Wijesundara, K.; Rajeev, P. Ultra-high-performance fibre-reinforced concrete for rehabilitation and strengthening of concrete structures: A suitability assessment. *Buildings*, 2023, 13 (3), 614. https://doi.org/10.3390/buildings13030614

[31] Alshahrani, A.; Kulasegaram, S.; Kundu, A. Utilisation of simulation-driven fibre orientation for effective modelling of flexural strength and toughness in self-compacting concrete. *Construction and Building Materials*, 2025, 459, 139767. https://doi.org/10.1016/j.conbuildmat.2024.139767

[32] Smarzewski, P.; Barnat-Hunek, D. Property assessment of hybrid fiber-reinforced ultra-high-performance concrete. *International Journal of Civil Engineering*, 2018, 16 (6), pp. 593-606. https://doi.org/10.1007/s40999-017-0145-3

[33] Barr, B. I. G. et al. Round-robin analysis of the RILEM TC 162-TDF beam-bending test: Part 3—Fibre distribution. *Materials and Structures*, 2003, 36 (9), pp. 631-635. https://doi.org/10.1007/BF02483283

[34] Sümer, Y.; Öztemel, M. Investigation of the Effect of GFRP Reinforcement Bars on the Flexural Strength of Reinforced Concrete Beams Using the Finite Element Method. *Fibers*, 2025, 13 (9), 125. https://doi.org/10.3390/fib13090125

[35] Mohan, A.; Madhavi, T. C. A study on mechanical properties of inorganic binders used in textile reinforced concrete using artificial neural network. *Asian Journal of Civil Engineering*, 2024, 25 (6), pp. 4513-4527. https://doi.org/10.1007/s42107-024-01062-4

[36] Al-Osta, M. A. et al. Flexural behavior of reinforced concrete beams strengthened with ultra-high performance fiber reinforced concrete. *Construction and Building Materials*, 2017, 134, pp. 279-296. https://doi.org/10.1016/j.conbuildmat.2016.12.094

[37] Dawood, M. H.; Al-Asadi, A. K. Mechanical properties and flexural behaviour of reinforced concrete beams containing recycled concrete aggregate. *Scientific Review Engineering and Environmental Sciences (SREES)*, 2022, 31 (4), pp. 259-269. https://doi.org/10.22630/srees.4250

[38] Chen, Z. et al. Spalling resistance and mechanical properties of ultra-high performance concrete reinforced with multi-scale basalt fibers and hybrid fibers under elevated temperature. *Journal of Building Engineering*, 2023, 77, 107435. https://doi.org/10.1016/j.jobe.2023.107435

[39] Smarzewski, P. Mechanical properties and durability of ultra-high performance concrete containing steel fibers. *Composite Structures*, 2025, 371, 119471. https://doi.org/10.1016/j.compstruct.2025.119471

[40] Choi, D. et al. Mechanical properties of ultra-high performance concrete (UHPC) and ultra-high performance fiber-reinforced concrete (UHPFRC) with recycled sand. *International Journal of Concrete Structures and Materials*, 2023, 17, 67. https://doi.org/10.1186/s40069-023-00631-2

[41] Lande, I. et al. Full-scale production and material properties of ultra-high-performance fiber-reinforced concrete (UHPFRC) for rehabilitation of bridge decks in Norway. *Frontiers in Built Environment*, 2025, 11, 1570920. https://doi.org/10.3389/fbuil.2025.1570920

[42] Dziomdziora, P.; Smarzewski, P. Effect of hybrid fiber compositions on mechanical properties and durability of ultra-high-performance concrete: a comprehensive review. *Materials*, 2025, 18 (11), 2426. https://doi.org/10.3390/ma18112426

[43] Hasan, M.; Jamil, M.; Saidi, T. Mechanical properties and durability of ultra-high-performance concrete with calcined diatomaceous earth as cement replacement. *Journal of the Mechanical Behavior of Materials*, 2023, 32 (1), 20220272. https://doi.org/10.1515/jmbm-2022-0272

[44] Huang, L.; Chen, H; Shen, J. Status and Perspectives for Mechanical Performance of Cement/Concrete Hybrids with Inorganic Carbon Materials. *Buildings*, 2025, 15 (19), 3525. https://doi.org/10.3390/buildings15193525

[45] da Silva, M. L. et al. The influence of materials on the mechanical properties of ultra-high-performance concrete (UHPC): a literature review. *Materials*, 2024, 17 (8), 1801. https://doi.org/10.3390/ma17081801

[46] Patiño, J.; Galli, L.; Suraneni, P. Effects of different types of fibers and fiber mixes on fresh and hardened properties of ultra-high performance concrete. *Materials and Structures*, 2025, 58 (10), 361. https://doi.org/10.1617/s11527-025-02875-8

[47] Tian, X.; Fang, Z.; Shao, Y. Flexural Behavior and Design of Prestressed Ultrahigh-Performance Concrete Beams: Failure Mode and Ductility. *Journal of Structural Engineering*, 2025, 151 (9), 04025127. https://doi.org/10.1061/JSENDH.STENG-13830